Development and Flight Testing of a Meso-Scale Cyclopter

Conference Paper · January 2017

DOI: 10.2514/6.2017-2014

2 authors:

Carl Runco
Texas A&M University
13 PUBLICATIONS **24** CITATIONS
SEE PROFILE

Moble Benedict
Texas A&M University
31 PUBLICATIONS **246** CITATIONS
SEE PROFILE

Development and Flight Testing of a Meso-Scale Cyclocopter

Carl C. Runco[1] and Moble Benedict[2]
Texas A&M University, College Station, Texas, 77840

This paper describes the design, development and flight testing of a meso-scale cyclocopter. Weighing only 29 grams, the present vehicle is the smallest cycloidal rotor based aircraft ever built. Unlike the previous cyclocopters, the current prototype utilizes a novel, light weight (3 grams) cycloidal rotor design, with cantilevered blades, having semi-elliptical planform shape and no exposed rotor shaft. To minimize bending deflections the blades use a unique, lightweight (0.15 grams each) but high strength-to-weight ratio unidirectional carbon-fiber based structural design and are fabricated using a specialized manufacturing process. The cycloidal rotor design was chosen through systematic performance measurements conducted using a custom-built miniature three-component force balance. Based on experimental parametric studies, a 4-bladed rotor and symmetric blade kinematics with pitch amplitude of 45° provided the highest thrust and power loading (thrust/power) and was used in the final rotor design. The airframe is fabricated using a combination of carbon-fiber and state-of-the-art 3D printing techniques. The attitude control strategy utilizes a combination of rpm-control of the two cycloidal-rotors/tail-rotor and thrust vectoring of the cycloidal rotors. The control strategy is implemented on a custom-built 1.3 gram autopilot, which uses a closed-loop proportional-derivative controller for hover stability. The vehicle has been systematically flight tested by tuning the feedback gains and has demonstrated relatively stable hovering flight.

I. Introduction

OVER the past decade there has been increased interest in developing different types of micro-air vehicles (MAVs), largely because of the potential mission capabilities associated with small-scale flying devices. Such miniature, lightweight vehicles offer superior portability, rapid deployment capability, and feature a low radar cross section. MAVs can further support tactical military operations or explore environments that would otherwise be too dangerous for a human, such as surveillance and reconnaissance in the battlefield, biochemical sensing, fire and rescue operations, border surveillance, and traffic monitoring. With their reduced noise signatures and lower production costs, MAVs are poised to effectively accomplish any and all of these types of tasks. However, these missions often require flying conditions outside of the flight capabilities of current systems and factors such as gusts, confined spaces, and increased flight times are prohibitive barriers to most MAVs in use today. To overcome these difficulties, flying platforms need to be developed that can navigate through these scenarios and must be designed to exhibit high gust tolerance and the ability to operate in confined spaces. To date, many small, fixed-wing MAVs have been developed, however these types of flying devices are unsuitable for missions which require hovering/low-speed flight or tight turns and other demanding maneuvers. Rotorcraft, on the other hand, are much more suited for these flight regimes, with most vehicles employing single, coaxial, or multi-rotor configurations. The primary aerodynamic limitation of conventional rotor blade designs for use in MAVs is the reduced efficiencies at low Reynold's numbers (10,000–50,000), in particular, low values of maximum figure of merit of around 0.65 (Ref. 1,2). The reduced aerodynamic performance is caused by the large values of profile drag associated with thick boundary layer formations on the blades, large induced losses, and higher rotational and turbulent losses in the downstream wake of the rotating blades (Ref 3, 4). This demands that a more efficient, hover-capable propulsion method be investigated that can harness the potential of low Reynold's number unsteady aerodynamics, while simultaneously providing the maneuverability and gust tolerance required of MAVs.

A promising solution to overcoming the deficiencies associated with standard rotors is the cycloidal rotor, or cyclorotor. The cycloidal rotor is a revolutionary vertical take-off and landing (VTOL) propulsion concept, and

[1] Graduate Research Assistant, Aerospace Engineering, 3141 TAMU, Student Member.
[2] Assistant Professor, Aerospace Engineering, 3141 TAMU, Member.

consists of several blades that rotate about a horizontal axis with the blade span parallel to the axis of rotation (Fig. 1). The pitch angle of each of the blades is varied periodically as the blade moves around the azimuth of the rotor such that the blade is at a positive geometric angle of attack both at the top and bottom halves of its circular trajectory. The blade kinematics and aerodynamic forces on a functioning cycloidal rotor are shown schematically in Fig. 2. Here, θ is the pitch angle, ϕ represents the direction of resultant thrust vector from vertical, and Ω is the rotational speed of the rotor. By varying both the rotational speed and the cyclic pitch phasing, the magnitude and direction of the net thrust vector of the rotor can be carefully controlled.

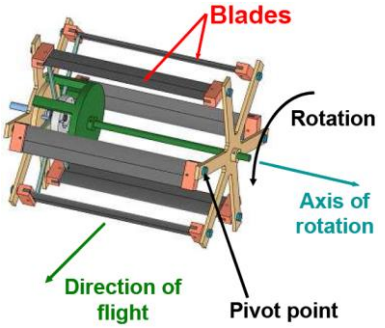

Figure 1. Cycloidal rotor model with key components identified.

There are several advantages of the cycloidal rotor over conventional rotors, one of the most significant of them being the fact that all the spanwise elements of the blade operate at the same aerodynamic conditions, which allows all the blade elements along the blade span to be set at optimum condition. This is in contrast with conventional rotors, in which each blade element along the span experiences a different flow velocity, Reynold's number, and angle of attack. Recent experiments conducted at the University of Maryland by the co-author have also shown that a cycloidal rotor may be more aerodynamically efficient in terms of power loading (thrust per unit power) than a conventional rotor of the same scale and similar actuator area (Ref. 5, 6). Also, a cycloidal rotor is able to obtain the required thrust at a significantly lower rotational speed than an equivalent conventional rotor, and therefore has a reduced acoustic signature, making it further advantageous for indoor reconnaissance missions. Additionally, since the blades are cyclically pitched once per revolution (1/rev), unsteady flow mechanisms may delay blade stall onset and in turn may augment the lift produced by the blades. Finally, since the thrust vector of a cycloidal rotor can be instantaneously set to any direction perpendicular to the rotational axis, the concept may also have better maneuverability compared to a conventional rotor based MAV, further demonstrating its usefulness in highly constrained applications and indoor operations.

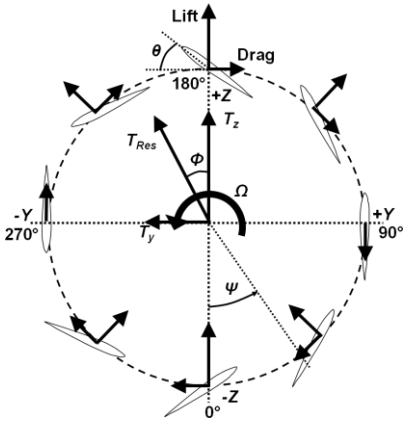

Figure 2. Blade kinematics and forces on a cycloidal rotor in hover.

The concept of the cycloidal rotor has been around for nearly a century, and many attempts, predominantly at full-scales, have been made to develop a cycloidal rotor based aircraft (Ref. 7-9). However, none of these vehicles were able to achieve flight because of the lower rotor performance (due to lack of understanding of the physics of the problem) and the large structural weight of the full-scale cycloidal rotors. Note that the cycloidal rotor might not be suited to full-scale aircraft applications anyway, and instead is more appropriate for MAVs where the design benefits from the inherent increase in strength-to-weight ratio as structures are scaled down. Now, with the advent of lightweight materials and electronics, improved manufacturing methods, and the development of high-efficiency motors, the cycloidal rotor concept has finally flown recently, proving the technique is possible with MAV-scale rotorcraft (Ref. 10-12). These vehicles, a sampling of which is shown in Fig. 3, have been developed and systematically studied by the co-author in order to optimize the performance of an MAV-scale cycloidal rotor (Ref. 11, 12). The experimental and computational studies have included detailed performance measurements, flowfield studies using Particle Image Velocimetry (PIV) (Ref. 10, 13-16), and the development and validation of an aeroelastic model to predict the hover performance of a cyclorotor (Ref. 17). These results have veritably shown that the cyclorotor is a viable propulsion device for hover-capable MAVs.

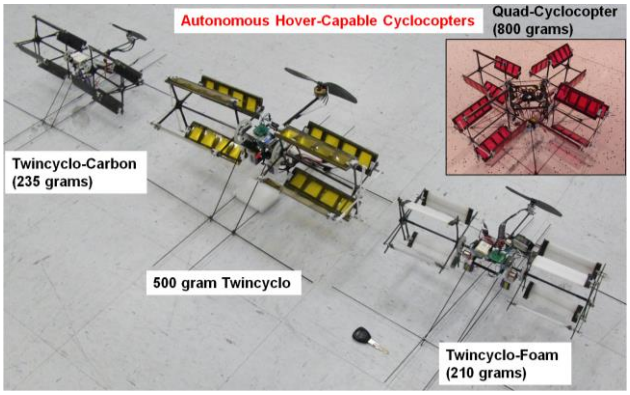

Figure 3. Hover-capable cyclocopters developed by the co-author, ranging in size from ~200 to 800 grams.

The previous vehicles developed have been in the 200-800 gram range, which is far outside the envisioned weight range of the initial MAV concept, which was approximately 100 grams gross take-off weight (Ref. 18). The focus of the present work, therefore, is to push the limits of current state-of-the-art technologies to design, build, and flight test the world's smallest

cyclocopter, targeted to be an order of magnitude smaller than smallest cyclocopter in existence today. The focus of the present study, therefore, is to develop and experimentally validate a meso-scale cycloidal rotor aircraft capable of greater maneuverability, stealth capability, and portability, beyond that offered by the larger-scale cyclocopters. This meso-scale cyclocopter, envisioned to be a versatile hand-held flying device, is shown conceptually in Fig. 4. Developing such an unconventional vehicle at these small scales is a brand new challenge not only from a vehicle design/construction standpoint, but also because it requires more fundamental research to be conducted to understand the 3-dimensonal unsteady aerodynamics (due to the low aspect ratio of the blades and high reduced frequencies) at ultralow Reynolds numbers experienced by the blades. Also, at small scales, owing to the lower inertia, vehicle dynamics tends to be much faster requiring high-bandwidth closed-loop control with very minimal actuator delays.

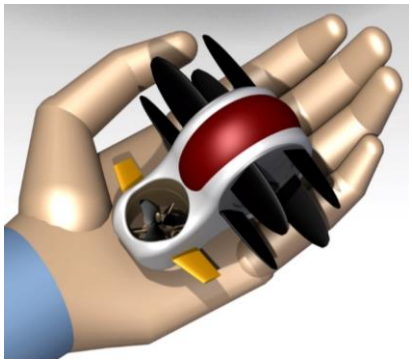

Figure 4. Conceptual drawing of a future meso-scale cyclocopter.

II. Vehicle Configuration

The current vehicle has a pair of miniature 1-inch radius cycloidal rotors, each weighing 3 grams total and capable of producing more than 10 grams of thrust, shown in Fig. 5. The current vehicle is shown in Fig. 6 with key components labeled. In this configuration, the vehicle is called a twin-cyclocopter. A conventional tail rotor and motor are incorporated in order to counteract the nose-up reaction pitching moment produced by the two cyclorotors rotating in the same direction, as well as provide an additional amount of lift for the vehicle. The rotational speed of the two cycloidal rotors and the tail rotor, combined with the ability to vector the thrust of the cyclorotors, gives the vehicle, in its current configuration, 5 control degrees of freedom (Ref. 11, 12), which results in the cyclocopter having greater actuation potential than a typically under-actuated system such as a quad-rotor. This means that the cyclocopter will be able to command instantaneous accelerations in more directions than a quad-rotor; therefore, the control authority and superior maneuverability have to be systematically investigated in order to fully reap the benefits and superior flying qualities offered by this type of thrust generating system. An airframe was developed using 3D printed parts and carbon fiber to integrate the rotors, tail prop and electronics into a single unit, resulting in a vehicle weighing 29 grams. A weight breakdown of the subsystems of the vehicle is provided in Table 1. The final vehicle is a twin meso-scale cyclocopter capable of both hovering and forward flight.

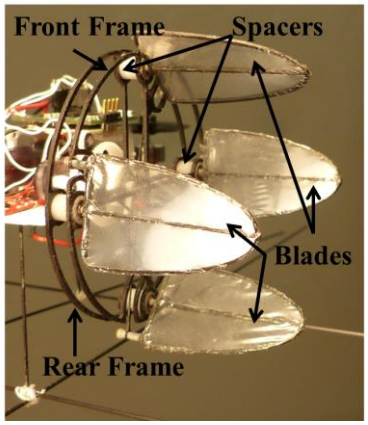

Figure 5. Meso-scale cycloidal rotor.

The remainder of this paper outlines the detailed design and experimental testing of the cyclorotors to evaluate the performance and choose an optimal blade and rotor design, which can generate the required thrust efficiently. The manufacturing process, developed specifically for creating strong, lightweight blades and rotor is explained in detail. Next, the vehicle control and stabilization techniques are described, as well as the vehicle telemetry and flight data collection. Finally, flight tests were conducted in hover, and the results are presented, which show the vehicle in relatively stable hovering flight, demonstrating successful vehicle operation.

III. Rotor and Pitch Mechanism Design

As stated previously, designing a light-weight cyclorotor with simplified blade-pitch mechanism is a challenge at small scales. Using knowledge gained from previous studies, a light-weight cyclorotor was designed that is different from any previously built cyclorotor. The rotor (shown in Fig. 5) uses cantilevered blades with a semi-elliptical planform shape to reduce rotor weight (by eliminating the shaft and the additional tip end-plate) and improve aerodynamic efficiency (by reducing induced drag). As a baseline

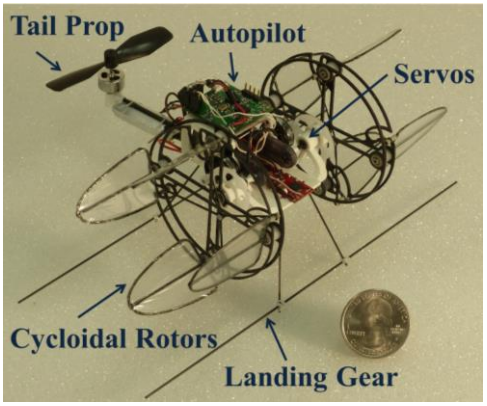

Figure 6. 29 gram meso-scale twin-cyclocopter.

design, a rotor radius of only one inch was chosen in order to keep the size and weight of the rotor low, as well as reduce the overall cross-sectional profile of the craft and thus fit well within the targeted vehicle size. The construction of rotors this small was challenging because they had to be lightweight, structurally stiff, and must accommodate the pitching mechanism. Because the blades on this current vehicle are cantilevered, it was not possible to simply scale down the structure of the rotor from previously built cyclocopters (shown in Fig. 3) and adopt it for use in this design. For this reason, a single-end-plate-based rotor was developed, which was designed to resist flexing under the centrifugal loads experienced during high-speed rotation. As shown in Fig. 5, the endplate was made of two separated carbon fiber frames connected with spacers made from Delrin® which also house the two root pitch bearings for each blade. This resulted in a lightweight end-plate with high stiffness.

Component	Weight (g)	Total (%)
Motors + transmission	7	24
Cyclorotors (combined)	6	21
Structure + wires	5	18
Li-Po Batteries	4.9	17
Electronics	3.7	13
Tail rotor + motor	2.4	8
Total	29	100

Table 1. Component Weight Breakdown of Cyclocopter

The cycloidal rotor utilizes a passive blade pitching mechanism which is based on a 4-bar linkage system where the blade pitching is kinematically coupled to the rotation. More details on the operation of the blade pitching mechanism can be found in Ref. 11. The pitching mechanism presented its own set of unique challenges due to its small size. One of the important considerations in any cycloidal rotor configuration is the fact that the pitch linkages must be hinged to the pitch offset beyond the end of the main rotor shaft in order to avoid interfering with it. For this cantilevered rotor design, the blades were mounted on the front carbon fiber frame, resulting in a root offset for each of the blades from the end of the main rotor shaft by the Delrin® spacer (see Fig 5). This allows the pitching linkages to run in the space between the carbon fiber frames directly from the end of the main rotor shaft to the blades. By strategically positioning the pitching links between the frames in this manner, they are protected during vehicle crashes. The pitch links are made of unidirectional carbon fiber prepreg. They are manufactured using the same process used to make the blades, outlined in the following section. This process allows the production of parts of consistent quality that are too delicate to be fabricated with other methods. The resulting linkages weigh only 0.01 grams each, and, since all of the carbon fibers are aligned in the direction of loading, they are very strong in that direction. Bushings allow the blades to rotate freely and are made from PEEK plastic (for abrasion resistance). The central offset is made of Delrin® and is glued to the central shaft.

IV. Blade Design and Manufacturing

The hallmark of the current cycloidal rotor is the cantilevered blades, a design feature possible only at smaller scales due to the increase in strength-to-weight ratio as the structure is scaled down. The blade design is biologically inspired, utilizing a symmetrically pitched, flat-plate airfoil. This design was chosen because of the low operating Reynolds number of approximately 11,000, and because constructing an airfoil at these scales is too impractical to implement. For the blade geometry, a semi-elliptical planform was selected because it is known that this shape improves aerodynamic efficiency. Manufacturing these blades proved to be one of the most difficult tasks, and required developing a specialized fabrication technique that ensured consistency and reproducibility in creating strong, lightweight blades. The method developed to accomplish this was to employ a layup technique using a Teflon™ mold and silicone compress which resulted in the successful fabrication of stiff, light-weight blades. The Teflon™ material was chosen because it will not bond with the carbon fiber when heat treated and is heat resistant, but is still strong enough to maintain the mold shape under the clamping pressure.

First, a strip of unidirectional carbon fiber is laid into the Teflon™ mold so that it makes a complete loop. Then 0.7 mm diameter carbon fiber rods for the pitch axis and pitch link pegs are laid in their respective slots. The pitching axis of each of the blades is carefully positioned at exactly the chordwise center of gravity in order to reduce the pitching moment on the blades due to centrifugal loads. After that, another complete loop is made around the mold with the unidirectional strip so that the rods are sandwiched between layers of it. The result of this layering is shown in (Fig. 7). This is then layered, as shown in Fig. 8, and clamped tightly together. The aluminum plates evenly apply the clamping pressure. The flexible/heat-resistant silicone sheet transfers the pressure to the carbon fiber and pushes it into the mold without developing pressure points. The anti-stick/releasing film prevents the carbon fiber from bonding with the silicone.

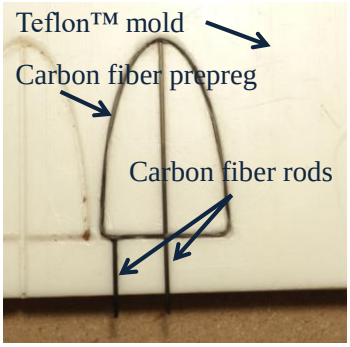

Figure 7. Carbon fiber frame in Teflon™ mold.

When the full mold layup is complete, it is cured at 350° F for 135 minutes. After the frame has cooled to room temperature, a 3 micrometer thick Mylar sheet is added to both sides of the now complete frame by applying contact cement in a very thin layer to the frame and then stretching the Mylar over it. A heating iron is used to remove any imperfections in the Mylar and adding tension to the frame. The resulting blades weigh less than 0.2 grams, and have a maximum chord of about 0.8 inches and a span of 1.3 inches.

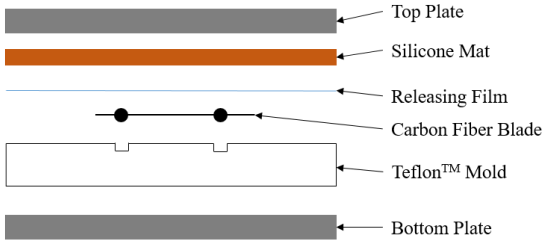

Figure 8. Constituitive layers of the blade layup.

V. Rotor Performance

In order to maximize the thrust and aerodynamic efficiency of the rotor design, a series of systematic experiments was conducted. These tests were to compare the performance of various rotor configurations. The pitch amplitude of the blade during the rotation of the rotor was varied from ±35° to ±50° in increments of 5° for blades of different size. The goal of this study was to obtain the blade size, pitch amplitude and number of blades that produces the highest thrust at a fixed rotational speed and best thrust/power ratio (or power loading) at the operating thrust. To accurately measure rotor performance (vertical force, sideways force, and power), a 3-component force balance was constructed and systematically calibrated to ensure accurate results. This new miniature 3-component force balance was used to measure the small forces produced by the 3 gram cycloidal rotors developed for the present vehicle. The complete force balance is shown in Fig. 9, with key components labeled. As can be seen, the balance is composed of force load cells that measure the two orthogonal components of thrust (T_Z and T_Y), and a reaction torque sensor that measures the torque generated by the rotor. In addition, a Hall-effect switch is used to measure the RPM of the rotor in real time. Mechanical power is calculated from the torque and rpm measurements.

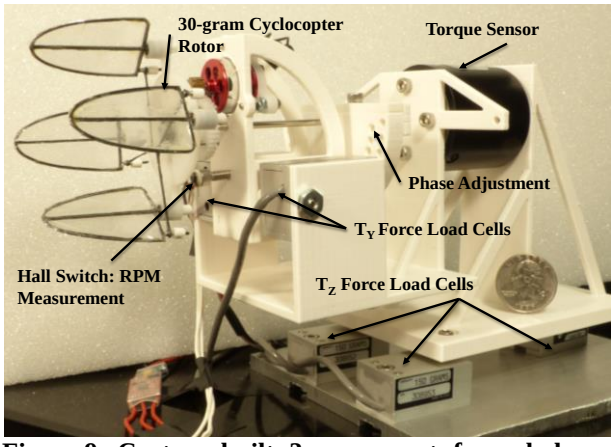

Figure 9. Custom built 3-component force balance for the meso-scale cyclocopter rotor.

The results from the experimental parametric studies using the 3-component balance are presented in the graphs below. The first step was to analyze the effect of blade size on rotor performance. The goal of comparing these different blade sizes was to explore which size would provide the maximum thrust for the lowest weight penalty. To this end, a set of three blades with identical planform, but scaled to different sizes, was built and tested. These blades were called Wing 1, Wing 2, and Wing 3, and are shown in Fig. 10. After testing, it was proven that Wing 3 was too heavy and therefore unable to withstand the inertial loads and it suffered from large deflections at the required RPM, so only limited data was collected at low rotational speeds. Wing 1, on the other hand, was lightweight enough to rotate at 4000 RPM, but was too small to generate sufficient thrust. Wing 2, however, was able to produce the necessary thrust at the targeted RPM, and was subsequently chosen as the final design. Fig. 11 plots the variation in thrust with rotational speed for Wing 1 and Wing 2, demonstrating that the larger wing can produce the required thrust at a reasonable rotational speed.

The rest of the studies were conducted using Wing 2 while changing other rotor parameters. Two different rotors, a 4-bladed and a 2-bladed rotor, were tested over the ±35° to ±50° range of pitching amplitude. A plot showing the variation in thrust with rotational speed for the 4-bladed pitch amplitude sweep of 35° to 50° is shown in Fig. 12. This graph conclusively shows that 45° maximum pitch amplitude generates the highest thrust for the 4-bladed rotor. These results are consistent with the previous findings that have found that large pitch amplitudes (40°–45°) produce the greatest amount of thrust, at least for larger-scale, 4-bladed cyclorotors (Ref. 19). Of equal importance is the thrust to power ratio (or power loading) plotted in Fig. 13, which is a quantitative metric describing the aerodynamic efficiency of the rotor. Again, the 45° pitch amplitude demonstrates superior performance relative to the other pitch amplitudes. The same set of sweep tests were done for

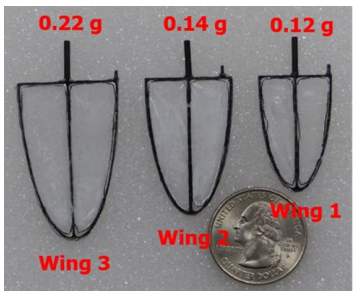

Figure 10. Three different blades tested.

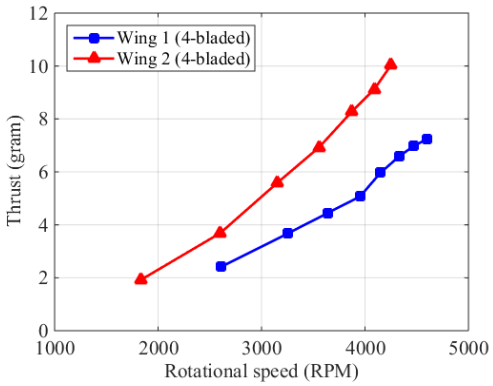

Figure 11. Thrust vs. rpm for two different wing sizes on a 4-bladed cycloidal rotor.

a 2-bladed rotor. The maximum thrust and power loading for the 2- and 4-bladed cases, achieved at 45° pitch amplitude, are plotted together in Figs. 14 and 15, respectively, which clearly shows the superior performance of the 4-bladed rotor.

It is interesting to note that on a 4-bladed rotor the 45° pitch amplitude had significantly higher performance than the 40° case; however, on a 2-bladed rotor both 45° and 40° had comparable performance. This is because the pitch amplitude alone does not fully reflect the aerodynamic conditions experienced by the blade. It is important to bring in the inflow through the rotor in each of the cases. Inflow velocity is proportional to the square root of thrust for a constant rotor area and it reduces the effective angle of attack seen by the blades. Since the 4-bladed configuration has a higher inflow than a 2-bladed one (due to higher thrust) at the same rotational speed, the effective angle of attack seen by the blade on a 4-bladed rotor is lower than the 2-bladed rotor. This means that the 45°, 4-bladed rotor may have an approximately equivalent angle of attack as the 40°, bladed one. This is also the reason why the 4-bladed rotor does not produce twice the thrust of the 2-bladed at the same rotational speed. Based on these results, a blade pitch amplitude of 45° and a 4-bladed rotor configuration was chosen as the final design. This rotor outperforms all of the other rotor configurations we tested and it produces the

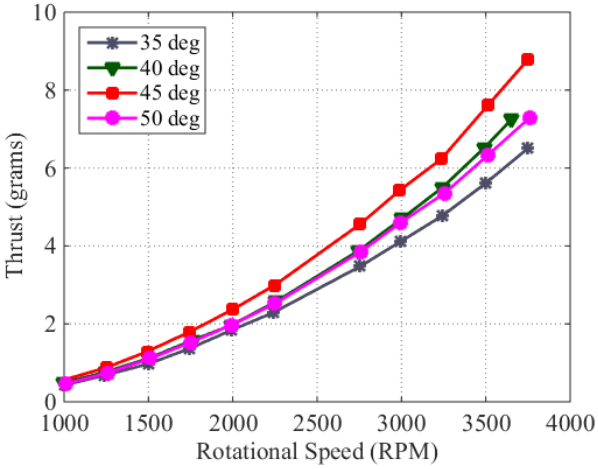

Figure 12. Thrust vs. rpm at different blade pitch amplitudes for 4-bladed cyclorotor.

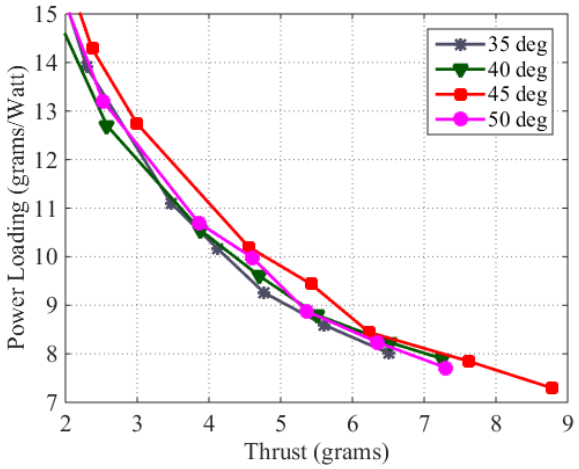

Figure 13. Power loading vs. thrust at different blade pitch amplitudes for 4-bladed cyclorotor.

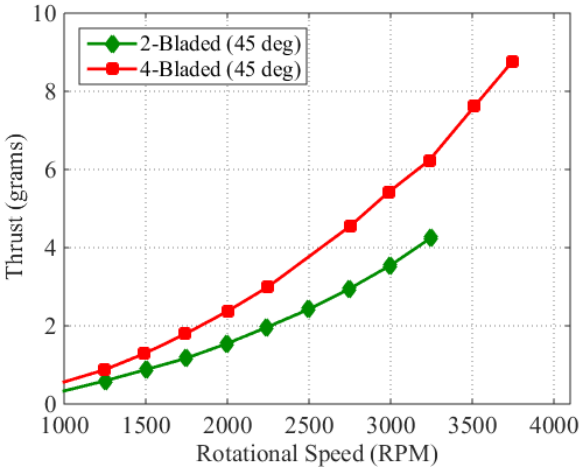

Figure 14. Comparison of thrust between 2-bladed and 4-bladed cyclorotors.

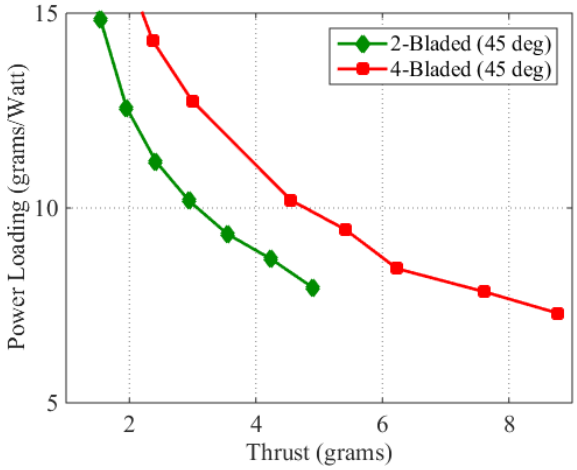

Figure 15. Comparison of power loading between 2-bladed and 4-bladed cyclorotors.

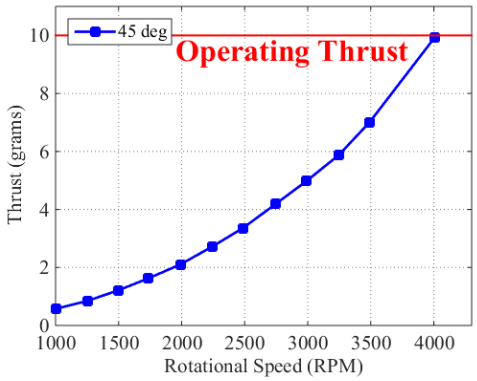

Figure 16. Thrust produced by final rotor design.

required thrust of 10 grams at our target operating RPM of about 4000, expending 1.28 watts of mechanical power, as shown in Figs. 16 and 17. A tail rotor is required to counteract the torque from the cyclorotors and augment the total thrust. A lightweight blade and motor was selected that can produce adequate thrust.

With blade size, geometry and number of blades systematically determined, the final analysis conducted on the blades and rotor setup was an evaluation of the blade deflection, either from a weak root boundary condition or bending along the span of the blade. The method used to qualitatively evaluate blade deflection was a series of experiments conducted using a strobe light, which was flashed in synchronization with the rotational frequency of the rotor. This gives the appearance that the rotor is stopped, and the amount of deflection experienced by the rotor was qualitatively compared with that of the non-rotating rotor. These results are shown in Fig. 18, and it can be clearly seen that when comparing the image with that of Fig. 5, there is only minimal deflection at the operating frequency of 4000 RPM. Based upon these results, it was concluded that, on the present rotor design, bending deflections do not substantially reduce rotor efficiency.

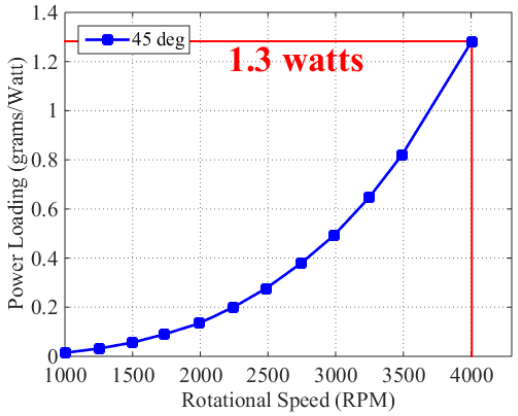

Figure 17. Power loading of final rotor design with mechanical power labeled.

VI. Vehicle Integration

Using two rotors in the configuration previously described, a flight-ready vehicle was constructed as previously shown in Fig. 6. Each component on the vehicle was carefully selected or manufactured to be as light as possible without compromising vehicle integrity. The airframe, which functions as an anchor point for all electrical and mechanical subsystems, is designed to hold the components in a compact configuration, thus, minimizing the profile of the craft. The airframe is rapid prototyped from ABS plastic and features carbon fiber rods extending outwards that function as landing gear. The thrust vectoring of each of the cyclorotors is actuated by means of a shape-memory alloy based servo actuator weighing 1 gram, the lightest possible COTS servo available. The rotors themselves are each driven by a 2.5 gram brushless, out-runner motor. Both the motors and actuator servos are powered by a 160mah single cell Li-Po battery weighing ~3.7 grams. The total weight of the first prototype is approximately 29 grams. Table 1, provided above, gives a breakdown of the system components by weight and Fig. 6 shows the completed vehicle.

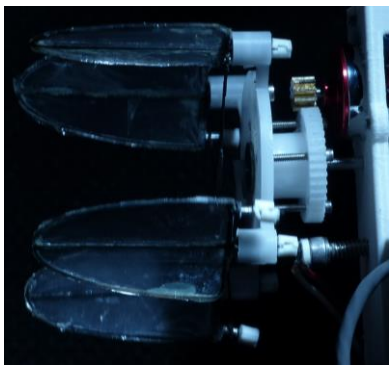

Figure 18. Blade deflection tests using strobe light duing rotor operating conditions.

VII. Attitude Control and Vehicle Telemetry

Control of the vehicle is accomplished in two ways: varying the RPM of the drive motors for either the main rotors or the tail prop (changes thrust magnitude) and rotating the offset link in the pitching mechanisms, which changes the blade pitch phasing (thrust vectoring). Modulating the rotor RPMs and cycloidal rotor pitch offset link angle provides complete control over rolling, pitching and yawing motion. Because of this ability to instantaneously change the magnitude and direction of the thrust vectors from the rotors, superior levels of agility and maneuverability can be achieved over traditional rotorcraft. The specifics of the control strategy implemented for attitude control are demonstrated in Fig 19. For roll control, the RPM of each of the main cyclorotors is changed differentially to create a moment about the longitudinal axis of the vehicle (Fig. 19a.). To control pitch, the RPM of the tail prop will be varied to generate a moment about the lateral axis due to the offset of the tail prop from the C.G. (Fig. 19b). Finally, yawing moments will be generated by rotating the pitch offset links which tilts the thrust vectors of the main rotors in opposite directions, creating a moment about the vertical axis of the vehicle (Fig 19c).

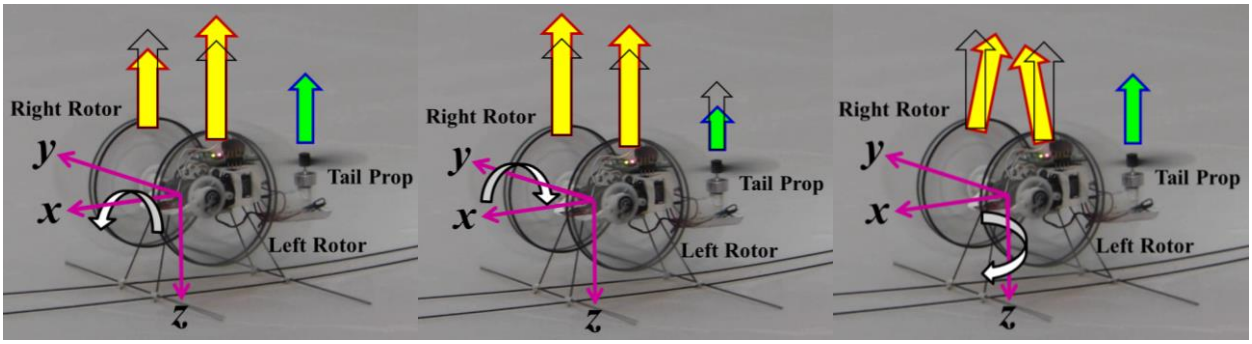

a) Positive roll control illustration of increased thrust on left rotor and decreased thrust on right cyclorotor.

b) Positive pitch control through increased thrust on main rotors and decreased thrust on tail prop.

c) Positive yaw control through forward thrust on left rotor and backwatd thrust on right rotor.

Figure 19. Implementation of control strategy for attitude control.

An important consideration of cyclocopter flight is the gyroscopic coupling present between roll and yaw degrees of freedom when either a roll or yaw control input is given. Because both main cycloidal rotors are rotating in the same direction (clockwise when viewed from the starboard side of the vehicle) about the lateral axis, any force which causes rotation of the vehicle about either the longitudinal or vertical axis will result in a gyroscopic moment 90° out of phase. Thus, if the vehicle is rolled, for example, to the right, a positive yawing motion (clockwise when viewed from above) will be introduced. To compensate for this coupled behavior between roll and yaw, the autopilot is programmed to automatically provide input commands to yaw when roll is activated, and vice versa. Feedback gains are handled similarly and provide coupled commands between both degrees of freedom. The result is a vehicle capable of many different types of flight regimes and maneuvering.

The attitude stabilization is implemented onboard using an autopilot – a custom-built, embedded processor-sensor board. It weighs 1.3 grams and is powered by a single 1-cell 3.7 volt 30mAh Li-Po battery. The autopilot houses an STM32 microprocessor with a 32-bit ARM Cortex M3 core for high-end onboard computation tasks. The MPU-9150 IMU integrated on the board includes tri-axial gyroscopes, accelerometers, and magnetometers. Wireless communications are serviced by an on-board nRF24L01 chip, a low-power 2.4 GHz RF transceiver. The autopilot has a sensor update rate of 500 Hz and is capable of streaming vehicle attitude data and actuator controls data to the base station with a short latency (Ref. 20). The autopilot is capable of sensing vehicle attitude and angular rates and sending corrective signals to the servos for stabilization by varying the pulse width input to the motors and servos.

To communicate wirelessly with the onboard controller, the operator uses a LabVIEW interface which includes a wireless IEEE 802.15.4 data link. The base station LabVIEW program allows the operator to control the vehicle, modify the feedback gains, change the sensitivity of pilot inputs, and record attitude data transmitted by the onboard processor. The LabVIEW program receives pilot inputs through the use of a commercially available DX6i Spectrum transmitter which is hardwired to the base station, and features a user interface to collect the feedback gains and pilot sensitivity specifications. The program then connects to the microcontroller through a wireless 2.4 GHz radio link and uses this connection to send the control inputs and receive the vehicle attitude and rates data. The data processing and inner-loop feedback control calculations are performed onboard by the microprocessor.

The on-board gyros measure the pitch (q), roll (p) and yaw (r) angular rates while the accelerometers record the tilt of the gravity vector in the body frame. The body-fixed frame directions and rates are sketched in Fig. 20. The vehicle attitude can then be extracted by integrating the gyro measurements with time. However, it is known that this leads to drift in attitude measurements (Ref. 21). Accelerometers on the other hand offer stable bias, but are sensitive to vibrations and in general offer poor high frequency information (Ref. 22). Therefore a complementary filter was incorporated to extract the pitch and roll Euler angles using a high-pass filter for the gyros (4 Hz cut-off) and a low-pass filter for accelerometers (6 Hz cut-off). The rotational vibrations were filtered out since they are sufficiently higher than the body dynamics. On-board inner loop feedback was implemented using a proportional-derivative (PD) controller as shown in Fig. 21. The feedback states are the pitch and roll Euler angles θ and ϕ, and the attitude rates, p, q and r. The outer loop feedback capability was provided for translational positioning by a human pilot or for a position tracking system.

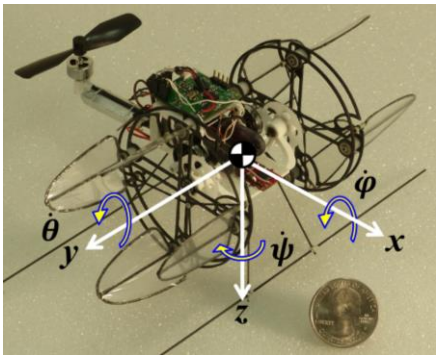

Figure 20. Micro cyclocopter body-fixed frame and with angular rates as measured by the on-board IMU.

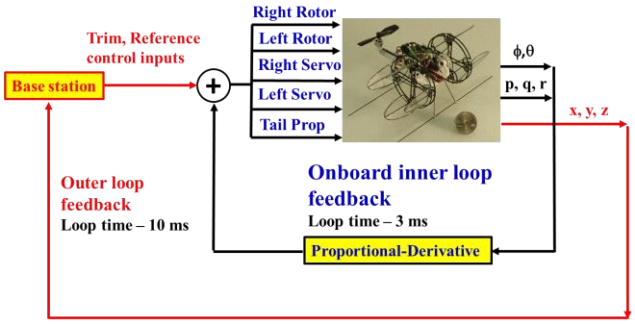

Figure 21. Diagram of closed - loop feedback implemented in control strategy.

VIII. Hovering Flight Testing

Since the flying qualities and behavior of this newly developed vehicle are largely unknown and initially unpredictable, an important flight testing consideration was safety of the vehicle during crashes in order to prevent destruction of the airframe and reduce maintenance requirements. For this reason, an *8ft x 8ft x 8ft* safe enclosure was utilized in which to conduct flight tests (Fig. 22). The sides are covered by a 90 micron thick plastic sheet to retain the vehicle in the enclosure during flying and offer a soft impact should the vehicle collide with the walls. Additionally, a sheet of plastic suspended from the edges of the frame a few inches off the ground provides protection to the vehicle in the case of a crash landing. As expected, flying in this enclosure substantially reduces the number of mechanical breakdowns and improves the efficiency of the flight testing operation. The vehicle takes off from the center of the suspended sheet which provides a stable platform for vehicle lift-off.

Figure 22. Safe-enclosure used for testing vehicle.

The feedback method used to stabilize the vehicle is an experimentally tuned PD controller which stabilizes the vehicle about a set point. Thus, it is important to trim the vehicle about the desired flight condition in order to appropriately utilize the controller feedback. For the initial flight tests, the desired flight condition was hovering flight. An important consideration for any flight regime is ensuring that the thrust vectors of the cyclorotors are vertical, which decouples the yaw and roll trim inputs. To accomplish this, the motor outputs were adjusted so that one rotor would spin much faster than the other. This rotor is then the primary source of lift for the vehicle and any yawing behavior the vehicle experiences is predominantly caused by the faster rotor. By observing the vehicle, we could adjust the trim of the appropriate servo until the vehicle no longer yawed. The servo was set to each extreme to ensure that there was enough control authority. Then the bisection method was used to converge on the point where the thrust vector was vertical. Once each rotor was adjusted in this manner the thrust vectors of the rotors were nearly vertical. The next step was to trim for eliminating roll. This was done simply by introducing a constant offset between rotor RPMs. Additionally, it was necessary to correct the throttle offset for the tail prop so as to ensure it generated enough thrust to balance out the moment generated by the spinning rotors and supplement the lifting force. After these steps were complete, the vehicle was tested by hopping it to make sure it lifted off vertically in a stable fashion. Minor adjustments (e.g. forwards and backwards trim, pitch, and roll) needed to be made to further trim the vehicle.

After successively trimming the vehicle for hovering flight, the next step was to introduce feedback gains in order to provide the additional level of control necessary beyond a human pilot's capability in order to stabilize the vehicle. The derivative gains had the effect of slowing down the vehicle dynamics and allowing us to further trim the vehicle. However, it was necessary to introduce proportional gains to eliminate drift. These were added in slowly until the vehicle behaved as expected, and then the derivative gains were slightly adjusted to improve hover stability. Shown in Figure 23 is a short, stable flight test conducted which successfully demonstrated the vehicle operation and flight testing procedure. The associated gyro data (Fig. 24) and Euler angles (Fig. 25) for this flight are provided. The onboard feedback control system was able to restrict the angular rates and the vehicle did not deviate from level flight by more than ±15 degrees in roll or pitch.

Figure 23. Meso-scale cyclocopter in relatively stable hovering flight.

IX. Conclusion

The cyclocopter concept, while having been conceived many years ago, has only recently seen materialization in the form of a fully functioning and operational micro air vehicle. The advantages of employing a cycloidal thrust generation mechanism instead of a traditional helicopter rotor include the possibility for much greater aerodynamic efficiency, agility, maneuverability, and gust tolerance. Thus, it is of great interest to reduce the size of the vehicle to the smallest scale possible for improved reconnaissance and surveillance

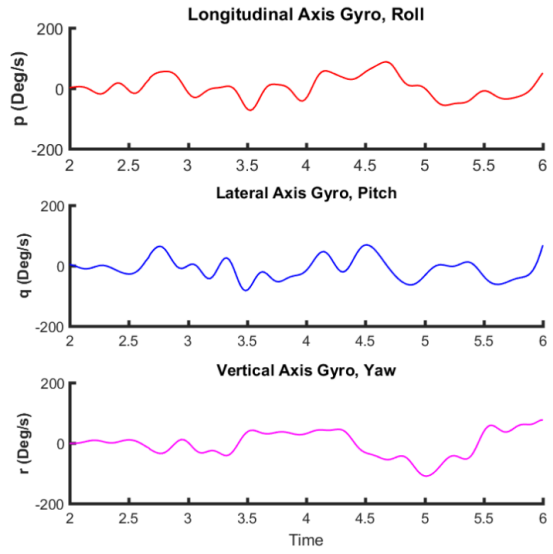

Figure 24. Angular rates for flight test.

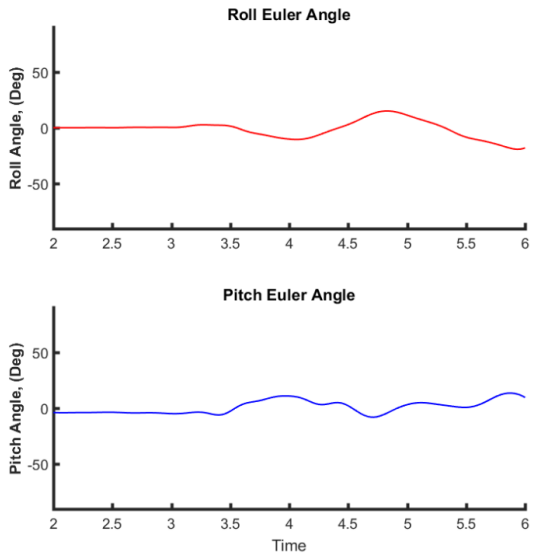

Figure 25. Euler angles of flight test.

for indoor scenarios. This paper has outlined the design, development, and flight testing of the world's smallest cycloidal-rotor based air vehicle. The first iteration of this cyclocopter has demonstrated that the concept can be created and implemented at small scales with careful designing and manufacturing. For this particular design, a cycloidal rotor with a single endplate and cantilevered, elliptical wings was developed. Through a systematic testing procedure, the blade design was optimized and a specialized manufacturing technique was created to reliably produce strong, lightweight blades. The present cyclorotors have a unique design, which takes advantage of the small scale to achieve higher thrust/weight ratios compared to previous cyclorotor designs. The blade manufacturing process developed in the present study allows ultra-lightweight blades to be fabricated with consistent quality and physical properties. Using the custom-built miniature 3-component balance developed, experimental parametric studies were conducted to optimize cyclorotor performance. Using an inner stabilization loop implemented on a custom-built onboard autopilot, the vehicle has been able to achieve relatively stable hovering flights. This demonstrated the downwards scalability of this revolutionary flying concept.

Immediate future work involves improving the flight qualities of the vehicle. Additionally, once the vehicle has achieved a greater level of flying quality with the on-board inner-loop attitude stabilization, a human pilot will be introduced in the outer-loop for position control with the goal of increasing the total flight capabilities of the vehicle. Once the endurance has improved, the next step is to extract a linearized state-space model of the vehicle through experimental system identification studies using a camera-based 3-D motion tracking system (i.e. VICON™). The motion capture system will also be used to replace the pilot in the outer loop with the purpose of flying the cyclocopter completely autonomously for an extended period of time. Thus the overall goal of the project is to develop an efficient meso-scale cyclocopter MAV (shown in Fig. 4) that could perform a stable, autonomous, 20-minute hover/forward flight indoors/outdoors, and even in the presence of moderate gusts.

Acknowledgments

This research was supported by the U.S. Army's Micro Autonomous Systems and Technology–Collaborative Technology Alliance (MAST-CTA) with Chris Kroninger (Army Research Laboratory–Vehicle Technology Directorate) as Technical Monitor.

References

[1] Pines, D., and Bohorquez, F., "Challenges Facing Future Micro-AirVehicle Development," Journal of Aircraft, Vol. 43, (2), March–April 2006, pp. 290–305.

[2] Chopra, I., "Hovering Micro Air Vehicles: Challenges and Opportunities," Proceedings of American Helicopter Society Specialists' Conference, International Forum on Rotorcraft Multidisciplinary Technology, Seoul, Korea, October 15–17, 2007.

[3] Leishman, J. G., Principles of Helicopter Aerodynamics, Cambridge University Press, New York, NY, 2006, pp. 229, 280, 334–337.

[4] Ramasamy, M., Johnson, B., and Leishman, J. G., "Understanding the Aerodynamic Efficiency of a Hovering Micro-Rotor," Journal of the American Helicopter Society, Vol. 53, (4), October 2008, pp. 412–428.

[5] Benedict, M., Jarugumilli, T., and Chopra, I., "Effect of Rotor Geometry and Blade Kinematics on Cycloidal Rotor Hover Performance," *Journal of Aircraft*, Vol. 50, (5), 2013, pp. 1340–1352.

[6]Benedict, M., Jarugumilli, T., and Chopra, I., "Experimental Optimization of MAV-Scale Cycloidal Rotor Performance," *Journal of the American Helicopter Society*, Vol. 56, No. 2, April 2011, pp. 022005-1 - 022005-11.

[7]Wheatley, J. B. and Windler, R., "Wind-Tunnel Tests of a Cyclogiro Rotor," NACA Technical Notes No. 528, May 1935.

[8]Kirsten, F. K., "Cycloidal Propulsion Applied to Aircraft," *Transactions of the American Society of Mechanical Engineers*, Vol. 50, No. AER-50-12, 1928, pp 25—47.

[9]Benedict, M., "Fundamental Understanding of the Cycloidal-Rotor Concept for Micro Air Vehicle Applications," Ph.D Thesis, Department of Aerospace Engineering, University of Maryland, College Park, MD, December 2010.

[10]Benedict, M., Jarugumilli, T., and Chopra, I., "Design and Development of a Hover-Capable Cyclocopter MAV," Proceedings of the 65th Annual National Forum of the American Helicopter Society, Grapevine, TX, May 27—29, 2009.

[11]Benedict, M., Gupta, R., and Chopra, I., "Design, Development and Open-Loop Flight Testing of a Twin-Rotor Cyclocopter Micro Air Vehicle," *Journal of the American Helicopter Society*, Vol. 58, No. 4, October 2013, pp. 1 – 10.

[12]Benedict, M., Shrestha, E., Hrishikeshavan, V., and Chopra, I., "Development of a Micro Twin-Rotor Cyclocopter Capable of Autonomous Hover," *Journal of Aircraft*, Vol. 51, No. 2, 2014, pp. 672 – 676.

[13]Sirohi, J., Parsons, E., and Chopra, I., "Hover Performance of a Cycloidal Rotor for a Micro Air vehicle," *Journal of the American Helicopter Society*, 52(3), July 2007, pp. 263—279.

[14]Benedict, M., Ramasamy, M., Chopra, I., and Leishman, J. G., "Performance of a Cycloidal Rotor Concept for Micro Air Vehicle Applications," *Journal of the American Helicopter Society*, Vol. 55, No. 2, April 2010, pp. 022002-1 - 022002-14.

[15]Benedict, M., Ramasamy, M., Chopra, I., and Leishman, J. G., "Experiments on the Optimization of the MAV-Scale Cycloidal Rotor Characteristics Towards Improving Their Aerodynamic Performance" Proceedings of the International Specialists' Meeting on Unmanned Rotorcraft, Scottsdale, Arizona, January 20—22, 2009.

[16]Benedict, M., Jarugumilli, T., and Chopra, I., "Experimental Performance Optimization of a MAV-Scale Cycloidal Rotor," Proceedings of the AHS Specialists' Meeting on Aeromechanics, San Francisco, CA, Jan 20—22, 2010.

[17]Benedict, M., Mattaboni, M., Chopra, I., and Masarati, P., "Aeroelastic Analysis of a Micro-Air-Vehicle-Scale Cycloidal Rotor in Hover," *AIAA Journal*, Vol. 49, No. 11, November 2011, pp. 2430 – 2443.

[18]McMichael, J. M., and Francis, USAF (Ret.), C. M. S., "Micro Air Vehicles Toward a New Dimension in Flight," *U.S. Department of Defense Weapons Systems Technology Information Analysis Center (WSTIAC) Newsletter*, Vol. 1, No. 13, JanJul 2000 Originally published online at http://www.darpa.mil/tto/MAV/mav auvsi.html, Aug. 7, 1997.

[19]Benedcit, M. and Chopra, I., "Design and Development of an Unconvnetional VTOL Micro Air Vehicle: The Cyclocopter," *Proceedings of SPIE Micro- and Nanotechnology Sensors, Systems, and Applications IV*, 83731F, International Society for Optics and Photonics, Baltimore, 2012.

[20]Hrishikeshavan, V., Chopra, I., "Refined Lightweight Inertial Navigation System for Micro Air Vehicle Applications," AHS Specialists' Meeting on Unmanned Rotorcraft and Network-centric Operations, Chandler, AZ, Jan 20-22, 2015.

[21]Georgy, J., Noureldin, A., Korenberg, M., and Bayoumi, M., "Modeling the Stochastic Drift of a MEMS-Based Gyroscope in Gyro/Odometer/GPSIntegrated Navigation," *IEEE Transactions on Intelligent Transportation Systems*, Vol. 11, (4), Dec 2010, pp. 856–872.

[22]Thong, Y. K., Woolfson, M. S., Crowe, J. A., Hayes-Gill, B. R., and Challis, R. E., "Dependence of inertial measurements of distance on accelerometer noise", *Measurement Science and Technology*, Vol. 13 , (8), pp.1163–1172 , 2002.